Acta Biomaterialia 88 (2019) 149–161

Contents lists available at ScienceDirect

Acta Biomaterialia

journal homepage: www.elsevier.com/locate/actabiomat

Full length article

The role of tissue remodeling in mechanics and pathogenesis of abdominal aortic aneurysms

Justyna A. Niestrawska [a], Peter Regitnig [b], Christian Viertler [b], Tina U. Cohnert [c], Anju R. Babu [a], Gerhard A. Holzapfel [a,d,*]

[a] Institute of Biomechanics, Graz University of Technology, Stremayrgasse 16/2, 8010 Graz, Austria
[b] Institute of Pathology, Medical University of Graz, Neue Stiftingtalstraße 6, 8010 Graz, Austria
[c] Clinical Department of Vascular Surgery, Medical University of Graz, Austria
[d] Norwegian University of Science and Technology (NTNU), Department of Structural Engineering, 7491 Trondheim, Norway

ARTICLE INFO

Article history:
Received 3 November 2018
Received in revised form 3 January 2019
Accepted 31 January 2019
Available online 5 February 2019

Keywords:
Abdominal aortic aneurysm
Collagen fiber dispersion
Second-harmonic generation imaging
Mechanical testing
Neo-adventitia

ABSTRACT

Arterial walls can be regarded as composite materials consisting of collagen fibers embedded in an elastic matrix and smooth muscle cells. Remodeling of the structural proteins has been shown to play a significant role in the mechanical behavior of walls during pathogenesis of abdominal aortic aneurysms (AAA). In this study, we systematically studied the change in the microstructure, histology and mechanics to link them to AAA disease progression. We performed biaxial extension tests, second-harmonic generation imaging and histology on 15 samples from the anterior part of AAA walls harvested during open aneurysm surgery. Structural data were gained by fitting to a bivariate von Mises distribution and yielded the mean fiber direction and in- and out-of-plane fiber dispersions of collagen. Mechanical and structural data were fitted to a recently proposed material model. Additionally, the mechanical data were used to derive collagen recruitment points in the obtained stress-stretch curves. We derived 14 parameters from histology such as smooth muscle cell-, elastin-, and abluminal adipocyte content. In total, 22 parameters were obtained and statistically evaluated. Based on the collagen recruitment points we were able to define three different stages of disease progression. Significant differences in elastin content, collagen orientation and adipocyte contents were discovered. Nerves entrapped inside AAA walls pointed towards a significant deposition of newly formed collagen abluminally, which we propose as neo-adventitia formation. We were able to discriminate two types of remodeled walls with a high collagen content – potentially safe and possibly vulnerable walls with a high adipocyte content inside the wall and significant amounts of inflammation. The study yielded a hypothesis for disease progression, derived from the systematic comparison of mechanical, microstructural and histological changes in AAAs.

Statement of Significance

Remodeling of the structural proteins plays an important role in the mechanical behavior of walls during pathogenesis of abdominal aortic aneurysms (AAA). We analyzed changes in the microstructure, histology and biomechanics of 15 samples from the anterior part of AAA walls and, for the first time, linked the results to three different stages of disease progression. We identified significant differences in elastin content, collagen orientation, adipocyte contents, and also a deposition of newly formed collagen forming a neoadventitia. We could discriminate two types of remodeled walls: (i) potentially safe and (ii) possibly vulnerable associated with inflammation and a high amount of adipocytes.

1. Introduction

Abdominal aortic aneurysms (AAAs) are local dilatations of the abdominal aorta. The bulge is weakening the vessel wall and appears predominantly in the elderly male population [1,2]. AAAs are usually clinically silent and may rupture eventually if not

* Corresponding author at: Institute of Biomechanics, Graz University of Technology, Stremayrgasse 16/2, 8010 Graz, Austria.
E-mail address: holzapfel@tugraz.at (G.A. Holzapfel).

https://doi.org/10.1016/j.actbio.2019.01.070
1742-7061/

treated [3]. The mortality rate in these cases lies around 85% [4]. Especially in older patients the treatment of AAAs with elective surgical repair does not necessarily improve survival [5]. Hence, a reliable, patient-specific prediction of rupture risk is needed to assess whether the risk of rupture justifies repair [6]. The current criterion for surgery is (still) the 'maximum diameter criterion', which is more a rule-of thumb than a scientific criterion [3,7]. Other criteria have been proposed such as the expansion rate [8], aneurysm asymmetry [9] or peak wall stress [10,11]. However, no criterion has been shown to be reliable so far. The study [12] suggested that a biomechanical patient-specific screening should be employed as finite element (FE) simulations are becoming more promising.

From a mechanical point of view, AAA rupture is a mechanical failure of the tissue once the peak wall stress exceeds the local strength [13]. As material properties depend significantly on the network of the extracellular matrix (ECM) including elastin and collagen, which are the primary load bearing proteins in the arterial wall [14]), changes in these components play a substantial role in pathogenesis. Therefore, a deeper understanding on the structure and ongoing reorganization during disease progression is essential. Studies which investigated wall stresses computationally were performed in, e.g., [15,3]. Such studies require physiological data on the material and structural level.

Over the past decade AAAs were studied widely especially mechanically. Biaxial extension tests in AAA were performed in, e.g., [16–19]. Studies, which performed uniaxial extension tests and reported a stiffer behavior in the circumferential direction were, e.g., [20–22], whereas [23–28] reported an increase in isotropy. Additionally, the pressure modulus was investigated as a mechanical parameter in [29,30]. On the basis of aortic porcine tissues the microstructure was linked to the mechanics to improve the outcome of FE simulations, see, e.g., [31]. Reorganization of collagen fibers during loading in cerebral aneurysms was analyzed in [32]. More recently we investigated the differences in the microstructure and mechanics between healthy aortic walls and AAA tissues [19]. Last but not least, the pathogenesis linked to material properties was investigated in several studies such as [16,33–36]. A correlation of the AAA diameter with collagen, smooth muscle cell (SMC), elastin content, the infiltration of inflammatory cells and the (uniaxial) rupture strength of 90 patients was reported in [28]. Specimens with higher diameters showed higher values of failure properties. However, there was no difference in strain when looking at the diameter and no other correlations were found either. However, the specific mechanical events leading to AAA development and eventually to rupture still remain unclear.

Elastin degradation seems to be accepted as one reason for the development of an aneurysmatic dilatation [37]. The study [38] investigated markers for elastin degradation linked to a pressure strain elastic modulus and found that elastin degradation correlates with increased wall distensibility and aneurysm formation. Data on changes in the collagen however is conflicting. Some authors report an increase in collagen fraction [39,40], while others report a reduction [41,33] or no change [42,43]. The order of pathological events leading to AAA initiation is not yet completely understood [44]. However, a consensus exists on the most important processes during the development of AAA, which are chronic inflammation, production of matrix degrading proteinases and their inhibitors [45]. Additionally, immunity seems to play a key role in aneurysm development [46]. After the dilatation caused by the loss of elastin, the adventitia is accepted to be the main load bearing part in the aortic wall. Eventually, collagen disruption seems to be the cause of rupture [45].

In our recent study [19] we observed significant amounts of adipocytes abluminally, covered by collagen within the wall, not adjacent to the outer side of the adventitia, as usually observed in healthy abdominal aortas [47]. Only two groups seem to have mentioned these entrapped adipocytes, e.g., [48–51] in AAA and [52] in transcranial aneurysms, but none investigated their influence on the mechanical behavior of the wall. However, the mentioned studies all hypothesized that adipocyte accumulations within the wall might be a key factor that causes wall degeneration and eventually rupture. In transcranial aneurysms, adipocyte accumulations were associated with SMCs and were hypothesized to originate from the thrombus or neo-vessels. In AAA studies on mouse models and human samples, [48–51] discovered that adipocyte like cells mostly accumulate in the abluminal side of the aneurysmal sac, but not in the neck. They noted that inflammation is associated with these adipocytes, but did not provide a hypothesis from where the adipocytes may originate from. The adipose tissue surrounding healthy vessels was mentioned in several studies such as [53,54], hypothesizing that this tissue could influence the pathogenesis within the adventitia of the adjacent vascular wall.

Adipocyte accumulations seem to be an important factor in the mechanical behavior of AAAs and motivated also the present study. To our knowledge it is the first one to systematically investigate the correlations between the mechanics, by utilizing biaxial extension tests, and the microstructure gained by second-harmonic generation (SHG) imaging and multiple histological parameters to define three stages of disease progression and therefore a hypothesis on the pathogenesis.

2. Materials and methods

2.1. Tissue preparation

Fifteen wall samples from (true) AAAs, with a median (interquartile range (iqr)) of 69 (65–77) years, 2 women and 13 men, were harvested from open aneurysm repair at the Department of Vascular Surgery, Medical University Graz, Austria. As during surgery, where a cut is made from the anterior side to place a graft, the smallest risk for the patient must be taken, only samples at the anterior side of the aneurysm could be obtained. The AAA samples were pieces with the axial direction marked by a surgical clip or suture and stored in Dulbecco's modified Eagle's medium at 4 °C until testing. As a representative control sample for histology one sample from an abdominal aorta with non-atherosclerotic intimal thickening was collected within 24 h of death and fixed in 4% formaldehyde solution (pH 7.4) during autopsy. All other data on healthy abdominal aortas relevant to this study were already collected and reported in our previous study [19].

The AAA tissue was cut into three separate samples, as indicated in Fig. 1. First, a rectangular sample with a size of approximately 15×5 mm with the long side marking the circumferential direction was prepared and fixed in 4% formaldehyde solution (pH 7.4) for histological analysis, as explained in Section 2.3. Subsequently a second rectangular sample, similar to the first one, was prepared for optical clearing, following the protocol in [55]. The specimens were dehydrated by means of a graded ethanol series consisting of $50, 70, 95\%$ and $2 \times 100\%$ ethanol solutions for each 30 min. The tissue was then cleared by submerging it

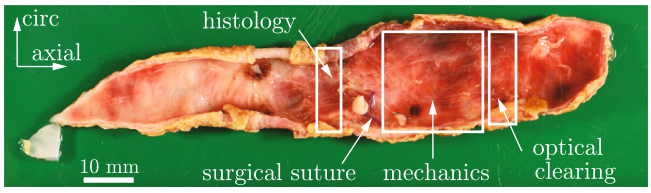

Fig. 1. Abluminal side of a representative AAA specimen showing the contours of the samples prepared for testing.

first into a benzyl alcohol benzyl benzoat (BABB) solution mixed with ethanol in the ratio 1 : 1 for 4 h [55]. Finally the specimens were placed in 100% BABB for at least 12 h before imaging as explained in Section 2.4. Finally a square sample with dimensions of 20 × 20 mm was prepared for mechanical testing, as explained in Section 2.5, and the circumferential direction was marked with a surgical marker.

2.2. Ethics

The use of AAA materials from human subjects was approved by the Ethics Committee of Medical University of Graz (27–250 ex 14/15). Participants gave informed consent prior to the inclusion in the study. The authors declare that the investigation conformed to the principles outlined in the Declaration of Helsinki.

2.3. Histology

Arterial segments, as indicated in Fig. 1, were fixed in 4% formaldehyde solution (pH 7.4), embedded in paraffin, sectioned at 3– 5 µm and stained. To visualize cells, hematoxylin and eosin (H&E) staining was used to evaluate the general cell content and architecture of the specimen and to estimate the inflammatory cell content and the calcification. Elastica van Gieson (EvG) staining was then applied to visualize elastin, collagen and SMCs. Additionally, small sections of two unfixed arteries were stained on cry-cut sections with Sudan Red G to confirm lipids inside voids seen within the wall.

2.4. Second-harmonic generation imaging

The three-dimensional (3D) collagen structure was determined by means of SHG imaging, which was performed on an imaging set-up consisting of a picosecond laser source and an optical parametric oscillator (OPO; picoEmerald; APE, Germany; HighQ Laser, Austria). These were integrated into a Leica SP5 confocal micorscope (Leica Microsystems Inc., Austria). The excitation wavelength was tuned to 880 nm and the detection of the signal was achieved using a BP 465/170 emission filter. 3D image stacks (z-stacks, 3 µm steps and cross-section images in $(x,y$-plane) were acquired using a Leica HCX IRAPO L 25 × 0.95 water immersion objective (working distance 2.5 mm for deep tissue imaging).

2.5. Mechanical testing

The samples were mounted into a biaxial testing device using hooks on surgical sutures. Subsequently the samples were submerged in a 0.9% saline solution and warmed up to 37 ± 1 °C. A stretch-driven protocol was used for testing, starting at a deformation of 2.5% and being increased by increments of 0.01 stretch until failure. As AAA tissue is very sensitive to initial preloads, zero strain was defined at a configuration of 0.05 N load. To cover a physiological range of deformations each sample was tested using five different stretch-ratios as follows: $\lambda_{\text{axial}} : \lambda_{\text{circ}} = 1:1$, $1:0.75, 0.75:1, 1:0.5$ and $0.5:1$, where λ_{circ} and λ_{axial} denote the stretch in the circumferential and axial directions, respectively. The samples were loaded quasi-statically with a rate of 3 mm/min. Normal and shear deformations were quantified following [56], and shear deformation was discovered to be negligible.

2.6. Material model

We assume that the aorta can be modeled as a purely elastic, incompressible and fiber-reinforced material. Therefore we introduce the deformation gradient $\mathbf{F}$ and the right Cauchy-Green tensor $\mathbf{C} = \mathbf{F}^{\mathrm{T}}\mathbf{F}$ [57], and define the strain-energy function Ψ according to [58]

$$\Psi = \Psi_{\text{g}}(\mathbf{C}) + \sum_{i=4,6} \Psi_{\text{fi}}(\mathbf{C}, \mathbf{H}_i) + p\mathbf{I}, \tag{1}$$

where Ψ_{g} represents the contribution of the ground matrix, i.e.

$$\Psi_{\text{g}}(\mathbf{C}) = \frac{c}{2}(I_1 - 3). \tag{2}$$

Herein I_1 is the first invariant, defined as $I_1 = \text{tr}\mathbf{C}$ and c is a material parameter, describing the stiffness of the ground matrix. The contribution Ψ_{fi} refers to the two fiber families defined by the two in-plane mean fiber directions

$$\mathbf{M}_4 = \cos\alpha\mathbf{e}_1 + \sin\alpha\mathbf{e}_2, \qquad \mathbf{M}_6 = \cos\alpha\mathbf{e}_1 - \sin\alpha\mathbf{e}_2, \tag{3}$$

where the fiber directions $\mathbf{M}_4$ and $\mathbf{M}_6$ make an angle α with the circumferential direction $\mathbf{e}_1$, while $\mathbf{e}_2$ indicated the axial direction. Additionally, the contribution of the fibers depends on the dispersion parameters κ_{ip} and κ_{op} (see [58]), which are incorporated into the generalized structure tensors $\mathbf{H}_4$ and $\mathbf{H}_6$ as follows:

$$\mathbf{H}_i = A\mathbf{I} + B\mathbf{M}_i \otimes \mathbf{M}_i + (1 - 3A - B)\mathbf{M}_{\text{n}} \otimes \mathbf{M}_{\text{n}}, \qquad i = 4, 6, \tag{4}$$

where $\mathbf{M}_{\text{n}}$ is a unit out-of-plane vector, and the constants A and B are given as

$$A = 2\kappa_{\text{op}}\kappa_{\text{ip}}, \qquad B = 2\kappa_{\text{op}}(1 - 2\kappa_{\text{ip}}). \tag{5}$$

This results in the definition of Ψ_{fi} as

$$\Psi_{\text{fi}}(\mathbf{C}, \mathbf{H}_i) = \frac{k_1}{2k_2}\left\{\exp[k_2(I_i^{\star} - 1)^2] - 1\right\}, \qquad i = 4, 6, \tag{6}$$

with the stress-like parameter $k_1 > 0$, the dimensionless parameter $k_2 > 0$ and the generalized invariants $I_i^{\star}$, defined as

$$I_i^{\star} = \text{tr}(\mathbf{H}_i\mathbf{C}) = AI_1 + BI_i + (1 - 3A - B)I_{\text{n}}, \qquad i = 4, 6. \tag{7}$$

Here, the invariants I_4, I_6 and I_{n} are defined according to

$$I_i = \mathbf{C} : \mathbf{M}_i \otimes \mathbf{M}_i, \quad i = 4, 6, \qquad I_{\text{n}} = \mathbf{C} : \mathbf{M}_{\text{n}} \otimes \mathbf{M}_{\text{n}}. \tag{8}$$

It is worth noting that the material model incorporates three material parameters (c, k_1, k_2), which can be determined by fitting the model to mechanical data (in this study obtained from biaxial tensile tests), and three structural parameters $(\kappa_{\text{ip}}, \kappa_{\text{op}}, \alpha)$, which can be determined by imaging (in this study obtained from SHG imaging).

2.7. Data analysis

2.7.1. Histological data

Histological investigation was performed on all samples to measure the wall thickness and the relative thickness of the individual layers in percent of the whole wall. All length measurements were performed on scanned slides using Aperio ImageScope (Leica Biosystems, Germany). The relative amount of lipids on the luminal and abluminal sides and the relative amount of calcification in percent of all constituents were quantified semi-quantitatively by two experienced pathologists. Additionally the relative elastin, SMC and the inflammatory cell contents were quantified.

2.7.2. Microstructural parameters

Images acquired by SHG imaging were analyzed by extracting data from z-stacks (3D images). Fourier power spectrum analysis and wedge filtering, as described in [55], were utilized to gain discrete angular distributions of relative amplitudes, resembling the fiber orientation. The fiber orientation was defined in the same manner, as introduced in [58,19], see, e.g., Fig. 2 in [19]. The underlying coordinate system was defined by the unit vectors $\mathbf{e}_1, \mathbf{e}_2$ and $\mathbf{e}_3$, representing the circumferential, axial and radial direction, respec-

tively. The general fiber direction **N** in the (unloaded) reference configuration was defined by the two angles $\Theta \in [0, 2\pi]$ (resembling the in-plane angle) and $\Phi \in [-\pi/2, \pi/2]$ (corresponding to the out-of-plane angle). Following [19] the in-plane and out-of-plane dispersions were fitted assuming their independence [59] with a bivariate von Mises distribution $\rho(\Theta, \Phi) = \rho_{ip}(\Phi)\rho_{op}(\Theta)$, defined as [58]

$$\rho_{ip}(\Phi) = \frac{\exp[a\cos 2(\Phi \pm \alpha)]}{I_0(a)}, \quad \rho_{op}(\Theta) = 2\sqrt{\frac{2b}{\pi}}\frac{\exp[b(\cos 2\Theta - 1)]}{\mathrm{erf}(\sqrt{2b})}, \tag{9}$$

where a and b are concentration (fitting) parameters defining the shape of the distributions, and $I_0(a)$ is the modified Bessel function of the first kind of order 0.

Following [58] two scalar quantities were introduced to measure the in-plane (κ_{ip}) and the out-of-plane (κ_{op}) dispersions by

$$\kappa_{ip} = \frac{1}{2} - \frac{I_1(a)}{2I_0(a)}, \qquad \kappa_{op} = \frac{1}{2} - \frac{1}{8b} + \frac{1}{4}\sqrt{\frac{2}{\pi b}}\frac{\exp(-2b)}{\mathrm{erf}(\sqrt{2b})}, \tag{10}$$

where and $I_1(a)$ is the modified Bessel function of the first kind of order 1 and $0 \leqslant \kappa_{ip} \leqslant 1$ and $0 \leqslant \kappa_{op} \leqslant 1/2$. A value of $\kappa_{ip} = 0.5$ corresponds to an isotropic fiber dispersion in-plane, whereas $\kappa_{ip} = 0$ resembles perfect alignment. For $\kappa_{op} = 0.5$ all fibers lie in-plane, whereas $\kappa_{ip} = 1/3$ corresponds to all fibers being dispersed out-of-plane.

2.7.3. Mechanical parameters

The model was fitted to all five testing ratios $(1:1, 1:0.75, 1:0.5, 0.75:1, 0.5:1)$ in both axial and circumferential directions simultaneously, utilizing the optimization toolbox `lsqnonlin` in Matlab [60]. The structural parameters κ_{ip}, κ_{op} and α were determined, as described in Section 2.7.2, and used for fitting the material model to the biaxial experimental data. Hence, the only three fitting parameters were c, k_1 and k_2. The goodness of fit was evaluated by the coefficient of determination R^2.

2.7.4. Inflection points

To compare the points of all stress-stretch curves where the collagen takes over the mechanical response, and hence the material stiffens rapidly, an 'inflection point' was defined. As mostly the circumferential direction behaved slightly stiffer, the inflection point was defined as the maximal change of slope of the circumferential 1 : 1 curve and calculated in Matlab.

For further analysis three distinct stages were defined: Stage 1 exhibiting an inflection stretch in the circumferential direction in a range of a healthy aortic wall, i.e. $1.10 \leqslant \lambda < 1.15$; stage 2 having a circumferential inflection stretch in the range of $\lambda \geqslant 1.15$; stage 3 exhibiting an inflection stretch $\lambda < 1.10$. The sample size of the groups was 6 for stage 1, 4 for stage 2 and 5 for stage 3.

The choice of the inflection point as the point of interest is supported by a recent study, which documents in vivo measurements of AAA strain ratios using 4D ultrasound [61]. The measured strain ratios varied in a range which is comparable to our measurements. Additionally, it is known that the ECM is degraded during AAA development, and hence the load bearing constituent which remains in the wall is mainly collagen. As the point where collagen starts bearing load is denoted by the inflection point we hypothesize that it is physiologically meaningful.

2.7.5. Statistics

All values are reported in medians and interquartile ranges (iqr), as a normal distribution could not be assumed due to the small sample cohort, and the outliers would affect the mean and the standard deviation. As we could not assume a normal distribution we used the Spearmans rank correlation to test for possible correlations between two independent data sets. Additionally, the Mann-Whitney U-test was utilized to test for significant differences between the data sets. Differences were considered statistically significant if the p-values for both tests were less than 0.05. All statistical analysis was performed using Matlab.

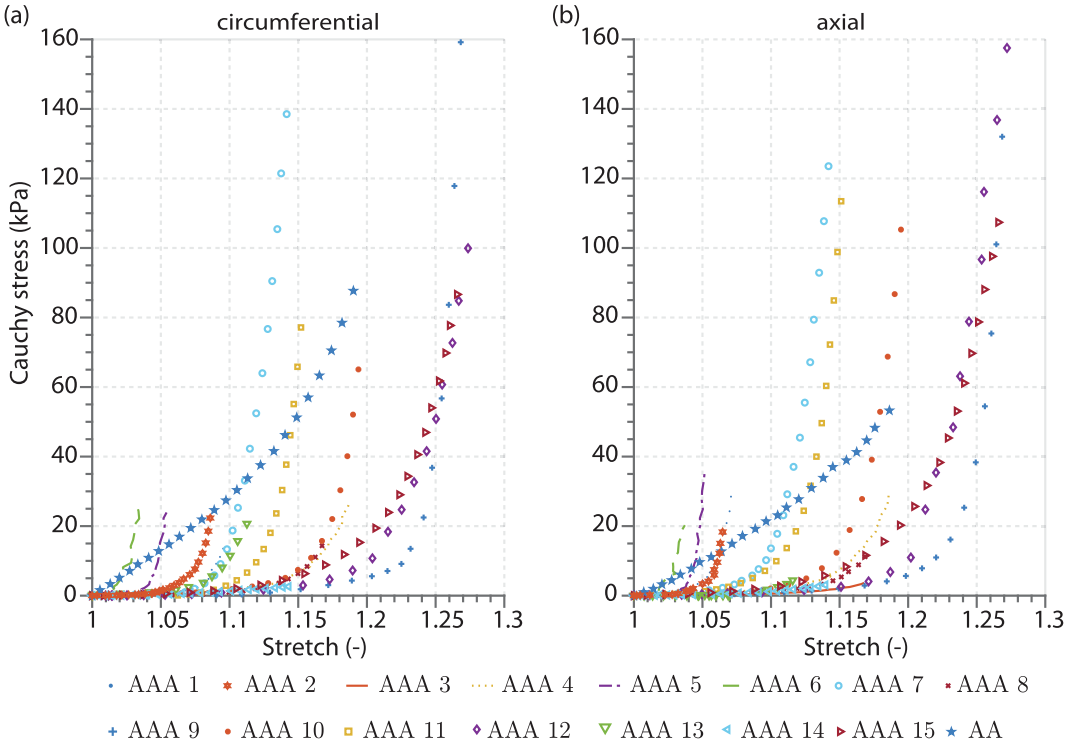

Fig. 2. Cauchy stress vs stretch behavior for 15 AAA samples and one AA control obtained from equibiaxial mechanical tests: (a) circumferential; (b) axial direction. The black circle indicates the exemplary 'inflection point' of sample AAA 11.

3. Results

3.1. Study population

All 15 samples were successfully analyzed for mechanical, microstructural and histological data. Table 1 summarizes all (potentially) relevant patient information. All aneurysms exhibited a maximum diameter of more than 55 mm, which is the size where a surgery is commonly advocated for men (50 mm for women, or if growth exceeds 5–10 mm per year) [2,62,63]. In addition, all AAA walls were covered by thrombus and did not originate from ruptured aneurysms. As statin intake might have an impact on adipocytes, we included that information as well.

Fig. 2 shows mechanical responses at a stretch ratio of 1 : 1 for all AAA and one healthy control sample (AA).

3.2. Healthy control

The healthy sample exhibited a circumferential inflection stretch of $\lambda = 1.12$, which is consistent with the study cohort in [19]. In healthy abdominal aortas three layers are present with a mean ratio of 20 : 49 : 31 (intima:media:adventitia) [55,19]. The SMC of the control sample was 35%, whereas the elastin content was 20%, both lying in the range of the reported contents [47]. The mean fiber direction of healthy abdominal aortas has a median (iqr) of $\alpha = 24.46^\circ$ (22.45–30.18°), showing very little dispersion out-of-plane (median (iqr)) $\kappa_{op} = 0.479$ (0.473–0.482°), as reported in [19].

Fig. 3 shows micrographs of the same sample location of a healthy abdominal aorta stained with (a) EvG and (b) H&E. The internal and external elastic lamina, thick elastin bundles and SMC are clearly distinguishable. Outside the adventitia loose connective tissue with a few adhering adipocytes can be seen.

The mechanical parameters, as reported in [19], were the following (reported in median (iqr)): $c = 11.59$ kPa (4.13–19.93 kPa), $k_1 = 2.66$ kPa (1.15–11.64 kPa) and $k_2 = 19.25$ (9.93–26.06). The c value indicates a pronounced initial stiffening, see the star-shaped curve in Fig. 2.

3.3. Inflection point related groups

Levels of disease progression were defined in three stages, depending on their 'inflection points', as described in Section 2.7.4, as

Table 1
Patient information of the 15 AAA specimen tested: number of specimen, age, gender (f: female, m: male), maximum diameter D, smoker, pack years, hypertension, diameters, statin intake, body mass index (BMI), – no information available.

#	Age (years)	Gender	D (mm)	Smoker y/n	Pack years	Hyper-tension	Diabetes y/n	Statin y/n	BMI
1	78	m	56	n	–	y	n	y	24.91
2	62	m	105	n	–	y	n	n	24.97
3	76	m	60	n	–	y	y	y	25.51
4	78	m	72	n	–	y	n	n	27.76
5	68	m	90	y	20	y	n	y	28.67
6	68	m	58	y	20	y	n	y	25.93
7	66	f	65	y	62.5	y	y	y	30.12
8	62	m	72	y	90	–	y	–	–
9	69	m	57	y	55	y	n	n	28.41
10	75	m	77	y	50	y	y	y	23.62
11	84	m	66	n	–	y	y	y	25.40
12	63	m	60	y	35	y	y	n	31.01
13	73	m	64	y	–	y	y	n	21.78
14	63	m	87	y	–	n	n	n	25.26
15	80	f	55	n	–	y	y	n	25.39

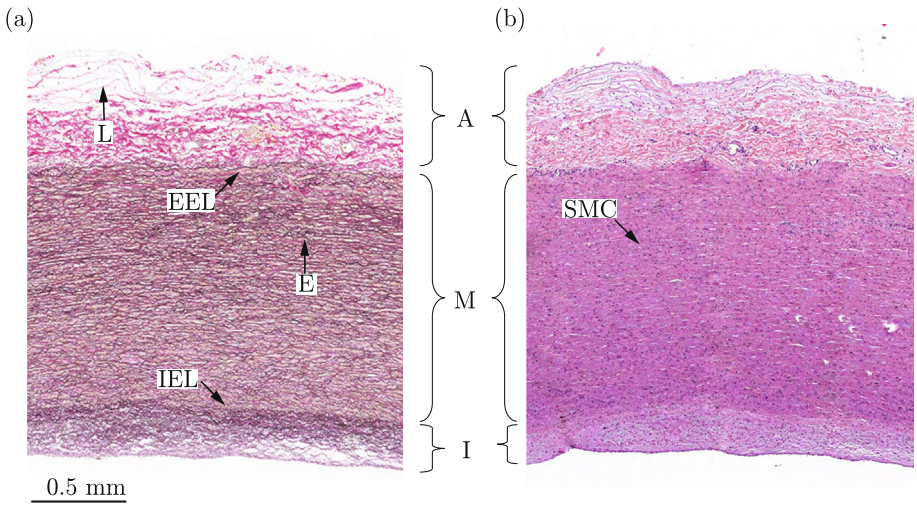

Fig. 3. Micrographs of the same location of the healthy control sample stained with; (a) EvG; (b) H&E. The three characteristic layers of the abdominal aortic wall (I: intima, M: media, A: adventitia) can be clearly seen. The EvG stain reveals the internal elastic lamina (IEL), the external elastic lamina (EEL), thick elastin bundles in brown (E) and collagen fibers in pink. Aidpocytes (L) are visible on the outer side of the adventitia. In the H&E stain SMC can clearly be seen in dark violet. In the outer part of the adventitia adipocytes from the surrounding fat tissue can also be identified.

Stage1 : $1.10 \leqslant \lambda < 1.15$, Stage2 : $\lambda \geqslant 1.15$,
Stage3 : $\lambda < 1.10$.

The choice of these groups was confirmed by significant differences in both circumferential and axial strains and stretches between all three groups ($p \leqslant 0.01$ for all cases).

3.3.1. Stage 1

The circumferential inflection stretch of the samples for stage 1 exhibited a median (iqr) of 1.12 (1.10–1.14). In all samples, three layers were present. However, the intima was thickened, resulting in a ratio between the layers of 40 : 30 : 30 (intima:media:adventitia). The elastin content decreased drastically to a median (iqr) of 3% (0.25–5%), as did the SMC content to a median of 3.5% (1.25–5%). A micrograph showing a AAA wall in stage 1 is shown in Fig. 4. The intima is notably thickened and neither IEL nor EEL are distinguishable anymore. Only a few elastic fibers (E) are visible in the middle of the wall, as well as SMCs. A small area with inflammatory cells (IF) is present in the surrounding adipose tissue. Worth noting is the following structure: a nerve (N) is visible inside the transition from the adventitia towards the loose connective tissue surrounding the vessel. Inside this loose tissue adipocytes (L) are also visible.

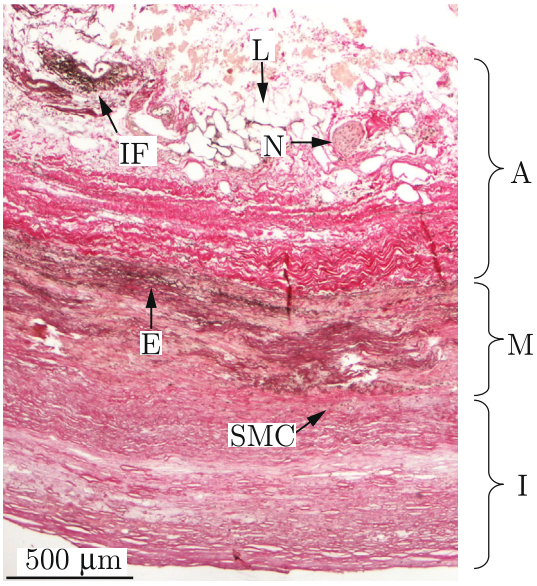

Fig. 4. EvG stained micrograph showing an AAA wall in stage 1. All three layers are visible. However, the intima (I) is significantly thickened in comparison to the healthy sample. Also the IEL and EEL are not clearly distinguishable anymore. A nerve (N) is visible on the outer part of the wall, as well as adipocytes (L) in the outer part of the adventitia (A). The media (M) contains notably less elastin fibers (E) and SMCa in comparison to the healthy sample. Also inflammatory cells (IF) are visible in the adventitia.

The left image of Fig. 5 shows a representative intensity plot for stage 1, where the red color identifies fiber angles at which there are fibers with that orientation, while the blue color indicates the absence of fibers. The abscises plots the angle of the fiber measured form the circumferential direction, i.e. 0°, while 90° refers to the axial direction. The plot shows fibers closely dispersed around the circumferential direction throughout the thickness. Indeed, the mean fiber angle for stage 1 is significantly smaller compared to healthy samples ($p < 0.001$) with a median (iqr) of 6.55° (5.19–11.62°). The out-of-plane dispersion increased to a value of $\kappa_{op} = 0.43$ (0.42–0.44), and the stiffness parameter k_2 increased by a factor of 2, compared to the healthy aorta, to a median (iqr) of 47.51 (24.92–60.41). Compared to the healthy aorta, especially the initial stiffness decreased significantly to $c = 0.59$ kPa (0.38–3.96 kPa), see also Fig. 2.

3.3.2. Stage 2

For stage 2 the inflection stretch in the circumferential direction showed a median (iqr) of 1.20 (1.20–1.22). In two samples only the adventitia was the only remaining wall part, whereas one exhibited two layers and one still all three. The elastin and SMC contents decreased to 1%, and the adipocytes located inside the wall (see Fig. 6) increased to 8.87% (4.39–13.17%) in comparison to no adipocytes present inside the wall in stage 1 or the healthy sample. Inflammation was visible on the abluminal side of the wall (IF), co-localizing with disrupted adipocytes (DL). Above the abluminal lipids, especially at locations showing inflammation, see Fig. 6, new collagen started to build up, forming a neo-adventitia (NA) (17.57% (8.78–49.38%) of the whole wall thickness). No such a layer could be identified in stage 1 or the healthy sample.

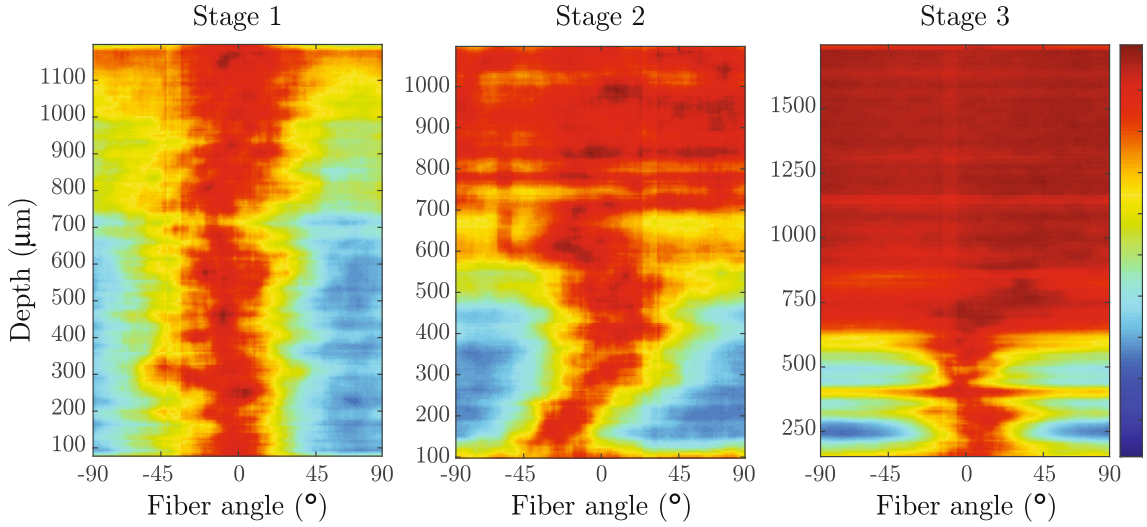

Fig. 5. Representative intensity plots for the three stages, showing the collagen fiber orientation and distribution through the depth of the aortic wall. A depth of 0 denotes the luminal side. Stage 1 shows fibers oriented closely towards the circumferential direction throughout the thickness of the wall. Stage 2 exhibits a similar fiber dispersion until a depth of around 600 μm, followed by a (more or less) isotropic fiber dispersion. Stage 3 shows the same tendency. However, the isotropic fiber distribution starts earlier and continues for over 1000 μm.

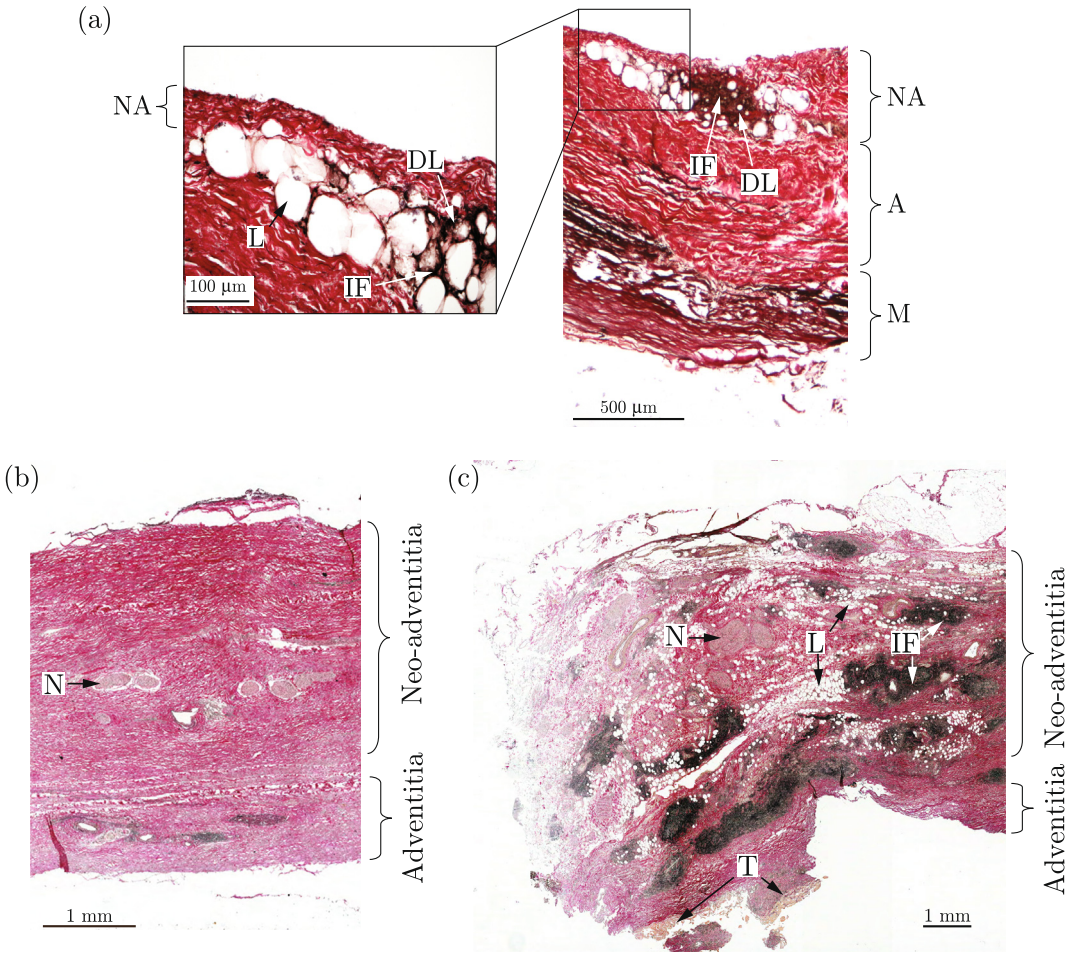

Fig. 6. EvG stained micrograph showing a AAA wall in (a) stage 2, (b) a 'safely' remodeled AAA wall and (c) a potentially vulnerable AAA wall in stage 3. In (a) no intima, elastin or SMCs are visible. The transition between media and adventitia is not clear. Inflammation (IF) is visible, located around disrupted adipocytes (DL). Non-disrupted adipocytes (L) are covered by apparently newly deposited collagen, the neo-adventitia (NA).Both samples in (b) and (c) show a significant neo-adventitia and neither media nor intima, the bottom denotes the luminal side. Nerves (N) appear entrapped within the wall in both samples, significant amounts of inflammation (IF), remnants of thrombotic material on the luminal side (T) and adipocyte cells (L) can be seen in (c).

The middle image of Fig. 5 shows a representative intensity plot for stage 2. Similar to stage 1, the fibers for the first 600 µm are aligned closely around the circumferential direction. However, the collagen fibers are isotropically dispersed further on, resulting in a median (iqr) angle of 33.11° (23.63–33.62°), being significantly bigger compared to stage 1 ($p = 0.02$).

3.3.3. Stage 3

The circumferential inflection stretch for samples in stage 3 had a median (iqr) of 1.05 (1.03–1.06). In all samples of stage 3 only one layer could be seen, except of one sample where the media and the adventitia were present. Hence, the amount of intima and media in stage 3 was significantly lower compared to stages 1 and 2. SMCs and elastin content were once more significantly decreased in comparison to stage 2, namely to 0% for all samples ($p = 0.01$). A significantly thickened neo-adventitia was present in the third stage with a median (iqr) of 66.22% (57.05–73.29%) of the wall ($p = 0.02$ to stage 1 but only $p = 0.08$ to stage 2).

By looking at the mechanical response, the third stage exhibited the stiffest behavior with a median (iqr) k_2 parameter of 636.29 (161.29–2142.10) ($p = 0.01$ compared to both stages 1 and 2). In addition, k_1 was significantly higher in comparison to stage 1 ($p = 0.05$) and slightly higher compared to stage 2 ($p = 0.09$) $k_1 = 8.96$ kPa (2.61–18.27 kPa).

Fig. 6 (b) and (c) shows two types of stage 3 walls. The wall in (b) shows the remains of the adventitia, followed by a dense collagen layer forming a neo-adventitia. The nerves (N) lie now inside the wall, emphasizing the thickness of the newly formed collagen. No inflammation can be seen on the abluminal side anymore, and no adipocytes can be seen anymore. The micrograph to the right, Fig. 6(c), shows another type of stage 3 wall: significant amounts of inflammation (IF) are visible throughout the wall, co-localizing with significant amounts of adipocytes (L). Again, a nerve (N) is entrapped in the middle of the wall, underlining the newly formed tissue on the abluminal side.

The right image of Fig. 5 shows a representative intensity plot for stage 3. Similar to stage 2, the luminal side shows fibers dispersed towards the circumferential direction, followed by a (more or less) isotropic fiber dispersion, which is more pronounced compared to stage 2. The out-of-plane dispersion was slightly higher compared to stage 1 ($p = 0.08$) with $\kappa_{op} = 0.402$ (0.379–0.412).

It is worth noting, that all patients except one took statins in stage 3, whereas no patient in stage 2 took these drugs. Two out of six patients in stage 1 took statins.

3.4. Statistical analysis

In total, 22 parameters were obtained by mechanical, microstructural and histological analyses; for a summary see

Table 2. Where reasonable, all these parameters were examined for correlations. A correlation was assumed significant when p-values were below 0.05. In total, 14 significant correlations could be identified, as shown in Table 3. Additionally, 6 pairs were identified to show a tendency towards a correlation (defined by a p-value > 0.05 and < 0.09), and were chosen to be shown since a correlation might motivate subsequent studies with a larger study cohort, see Table 4.

For example, SMC content (in %) vs percentage of newly built neo-adventitia of the wall correlate significantly, showing less SMC content in aortas with thicker neo-adventitia. Also the dimensionless stiffness parameter k_2 correlates significantly with the stretch λ_{IP} at the inflection point in the circumferential direction, where k_2 is very high for low λ_{IP}, while k_2 falls rapidly for higher λ_{IP}. The amount of neo-adventitia significantly increases with decreasing layers in the AAA wall.

Additionally to the grouping in inflection point groups, the samples were also grouped (yes/no) to examine the possible effects of diabetes and statin intake on the examined parameters. Patients with diabetes exhibited a significantly lower initial stiffness ($c = 1.16$ kPa (0.34–1.82 kPa)) compared to patients without diabetes ($c = 6.56$ kPa (2.11–6.83 kPa), $p = 0.04$). Interestingly, the stiffness parameter k_2 was significantly higher in patients without diabetes ($k_2 = 636.29$ (210.00–2142.10)) than in patients with diabetes ($k_2 = 43.86$ (17.79–48.75), $p = 0.007$).

Table 3
Significant correlations with corresponding p- and r-values. λ_{IP} = stretch at the inflection point in the circumferential direction; LL = luminal lipid deposits; BMI = body mass index. Intima %, media %, adventitia % and neo-adventitia % correspond to the percentage of the individual layer relative to the whole wall thickness.

Correlated variables	p-value	r-value
κ_{op} and k_2	0.000	0.79
λ_{IP} and k_2	0.022	−0.59
λ_{IP} and intima %	0.042	0.53
Intima % and elastin	0.049	0.52
Intima % and SMC	0.000	0.88
Media % and LL	0.030	0.56
Media % and elastin	0.001	0.77
Media % and SMC	0.000	0.92
Adventitia % and diameter	0.043	−0.53
Neo-adventitia and α %	0.050	0.51
Neo-adventitia % and SMC	0.003	−0.72
Neo-adventitia % and # layers	0.006	−0.68
Diameter and inflammation	0.018	0.60
BMI and LL	0.009	0.64

4. Discussion

In this study several correlations were discovered, which in the end enabled a definition of three stages of disease progression. For example, the dimensionless stiffness parameter k_2 was significantly correlated with the stretch λ_{IP} at the inflection point in the circumferential direction, showing a significantly stiffer behavior for low λ_{IP} with earlier collagen fiber recruitment. The parameter k_2 was also significantly correlated with the out-of-plane dispersion parameter κ_{op}, indicating a higher out-of-plane orientation with increased stiffness, and hence with disease progression. As the integrity of the AAA wall is lost when the ECM is degraded, collagen fibers are less aligned in-plane, consistent with our earlier study [19].

The mean collagen angle α, and the SMC content correlated positively with the relative thickness of neo-adventitia, indicating the

Table 2
22 parameters obtained by mechanical, microstructural and histological analyses of all AAA samples. Adv = adventitia; Neo-adv = neo-adventitia; Throm = thrombotic material; LL = luminal lipid deposits; Calc = calcification; Inflam = inflammatory cells; BMI = body mass index; λ_{IP} = stretch at the inflection point in the circumferential direction; σ_{IP} = associated Cauchy stress at the inflection point.

		Mechanical parameter			Structural parameter		
		c (kPa)	k_1 (kPa)	k_2 (–)	κ_{ip} (–)	κ_{op} (–)	α (°)
Stage 1	median	0.59	1.30	47.51	0.242	0.433	6.55
$n = 6$	[Q1;Q3]	[0.38; 3.96]	[0.48; 2.21]	[24.92; 60.41]	[0.234; 0.260]	[0.425; 0.441]	[5.19; 11.62]
Stage 2	median	1.83	0.46	17.79	0.224	0.455	33.11
$n = 3$	[Q1;Q3]	[1, 55; 2.54]	[0.40; 1.88]	[15.67; 30.83]	[0.219; 0.232]	[0.433; 0.463]	[23.63; 33.62]
Stage 3	median	3.78	8.96	636.29	0.224	0.402	22.90
$n = 6$	[Q1;Q3]	[0.78; 6.77]	[2.61; 18.27]	[161.29; 2142.10]	[0.191; 0.236]	[0.379; 0.421]	[18.41; 47.02]

		Histological parameter					
		Intima (%)	Media (%)	Adv (%)	Neo-adv (%)	Layer (–)	Throm (%)
Stage 1	median	46.37	17.09	30.78	0	3	2.50
$n = 6$	[Q1;Q3]	[32.31; 50.39]	[9.03; 24.25]	[19.04; 37.86]	[0; 11.86]	[3; 3]	[0; 8.75]
Stage 2	median	48.00	18.03	18.81	17.57	3	0
$n = 3$	[Q1;Q3]	[24.00; 48.67]	[9.01; 21.81]	[16.94; 22.60]	[8.78; 49.38]	[2; 3]	[0; 7.50]
Stage 3	median	0	0	33.78	66.22	1	0
$n = 6$	[Q1;Q3]	[0; 0]	[0; 0]	[26.10; 40.96]	[57.05; 73.29]	[1; 1]	[0; 1.50]

		Histological parameter					
		LL (%)	Calc (%)	Elastin (%)	SMC (%)	Collagen (%)	Inflam (%)
Stage 1	median	0	0	3.00	3.50	60.00	2.50
$n = 6$	[Q1;Q3]	[0; 7.50]	[0; 1.50]	[0.25; 5.00]	[1.25; 5.00]	[57.00; 61.50]	[0; 12.50]
Stage 2	median	2.00	15.00	1.00	1.00	60.00	2.00
$n = 3$	[Q1;Q3]	[1.00; 11.00]	[7.50; 17.50]	[0.50; 3.00]	[0.50; 3.00]	[54.50; 63.00]	[2.00; 6.00]
Stage 3	median	0	0	0.05	0	45.00	5.00
$n = 6$	[Q1;Q3]	[0; 0]	[0; 7.50]	[0; 0.78]	[0; 0]	[41.25; 75.00]	[1.25; 8.75]

		Inflection point			
		Diameter (mm)	BMI (–)	λ_{IP} (–)	σ_{IP} (kPa)
Stage 1	median	72.00	25.26	1.12	2.89
$n = 6$	[Q1;Q3]	[67.50; 75.75]	[23.62; 25.40]	[1.11; 1.14]	[2.38; 7.52]
Stage 2	median	57.00	28.41	1.20	17.38
$n = 3$	[Q1;Q3]	[56.00; 58.50]	[26.90; 29.71]	[1.20; 1.22]	[14.06; 19.93]
Stage 3	median	62.50	25.72	1.05	1.40
$n = 6$	[Q1;Q3]	[58.5; 83.75]	[25.11; 27.99]	[1.03; 1.06]	[1.19; 5.78]

Table 4
Pairs of parameters showing a tendency towards a correlation. λ_{IPc} = stretch at the inflection point in the circumferential direction; λ_{IPa} = stretch at the inflection point in the axial direction; media %, adventitia % and neo-adventitia % correspond to the percentage of the individual layer relative to the whole wall thickness.

	p-value	*r*-value
κ_{op} and λ_{IPa}	0.080	0.47
λ_{IPc} and media %	0.085	0.46
λ_{IPc} and SMC	0.077	0.47
λ_{IPc} and # layers	0.065	0.49
Intima % and calcification	0.066	−0.65
Diameter and calcification	0.086	−0.46

neo-adventitia as a marker of disease progression, as did the relative thicknesses of intima and media, which correlated significantly with elastin and SMC contents. A significant correlation with the diameter was found with the amount of inflammation, confirming findings in [64].

4.1. Hypothesis of a mechano-pathogenic model in three stages

Fig. 7 illustrates a flowchart depicting our hypothesis of disease progression, derived from observed changes in mechanics, histology and microstructure (collagen architecture). The chart starts with the characteristic mechanical behavior of a healthy aorta. Typically, the aorta shows a significant initial stiffness (see also Fig. 2, sample AA therein) (median (iqr) $c_{AA} = 33.86$ kPa (6.88–98.76 kPa)), and once it stiffens, the slope is rather moderate ($k_{2\,AA} = 19.25$ (9.93–26.06)), [19].

By looking at the histology, we can see a rather thin intima, a clear membrana elastica interna, and a clear membrana elastica externa, separating intima from media and media from adventitia, respectively. The media incorporates collagen and elastin fibers, and has a significant amount of SMCs. The adventitia exhibits a thicker, wavier type of collagen than the media, and nerves and adipocytes are visible on the outer side of the wall.

The typical collagen structure is depicted in the intensity plot to the right, taken from [19], showing a rather isotropic intima (starting from the bottom), followed by two counter-rotating collagen fiber families throughout the media, and finally two fiber families more aligned to the axial direction in the adventitia.

4.1.1. Stage 1

In several studies [65–68] it has been shown that a degradation of the extracellular matrix occurs, accompanied by a degradation of elastin and SMCs [69] (see Table 2) (for a theory of the initiation of aneurysm formation, see, e.g., [68,44]). As the elasticity of elastin is lost, an aneurysm starts to form [68]. Following the bulging, and due to lack of cells which might deposit new collagen, collagen fibers reorient passively towards the circumferential direction ($\alpha_{Stage\,1} = 6.55^\circ$ (5.19–11.62°)).

This is clearly visible in the intensity plot of stage 1 – all collagen fibers throughout the wall thickness are more or less oriented closely towards the circumferential direction. The point where collagen fibers get recruited is around the same stretch as in healthy samples. However, the initial stiffness decreases rapidly ($c_{Stage\,1} = 0.59$ kPa (0.38–3.96 kPa)), see, e.g., Fig. 2, sample AAA 11. The slope, once collagen gets recruited, is more pronounced, increasing to a value of ($k_{2\,Stage\,1} = 47.51$ (24.92–60.41)).

The intima starts to thicken, but most severely a significant loss in elastin and SMC content can be seen. As this leads to a loss of the membrana elastica interna and externa, a clear distinction between the layers becomes difficult (see also Fig. 4). Adipocytes and nerves are still located on the outer side of the wall, embedded in loose connective tissue.

We hypothesize that the growing aneurysm presses against the surrounding tissue, and hence compresses the perivascular adipose tissue, or 'tunica adiposa' [53]. Due to the pressure, adipocytes undergo in part a necrosis or an apoptosis, and the evading lipids are taken over by macrophages. This is a starting point for inflammation which accumulates inflammatory cells and fibroblasts, which further leads to the production of collagen fibers comparable to scar formation.

The study [54] states that perivascular adipose tissue might be linked to vascular disease, as adipocytes might contribute with a local toxic effect by migration of immune cells into the vascular wall. This might promote inflammation there, as obesity is associated with changes in adipokine secretion. Hence, the local pathogenic effect of a 'tunica adiposa' may be either direct by compression of the vessels or indirect by changes in fat tissue itself with diseases such as obesity [70,71]. Although the effect of perivascular fat remains incompletely understood, the mechanisms seem to include a direct effect on the vasculature such as the stimulation of immune cell migration into the vascular lumen [54].

4.1.2. Stage 2

We observed inflammation co-localizing with adipocytes in stage 2, which was not observed in healthy arteries or stage 1 AAAs. These inflammatory cells together with fibroblasts have the ability to deposit collagen [72]. As these cells are the only vital appearing cells we could localize in the AAA walls, we hypothesize that all collagen deposition is due to this inflammatory process on the abluminal side of the aorta. This theory is supported by the fact that a significant isotropically distributed layer is visible in the intensity plots of collagen orientation, which follows collagen fibers closely oriented towards the circumferential direction. As the aneurysm grows, stresses in the axial direction increase, and hence an isotropic fiber orientation of collagen appears, as also hypothesized in [73,28]. In addition, adipocytes and nerve cells covered by dense collagen fibers are already visible in micrographs of stage 2 AAA walls, see Fig. 6(a). We call this new deposition of collagen at the outer side of the AAA 'neo-adventitia'. Statistically significant differences in the mean fiber angle α and the thickness of the neo-adventitia further support this hypothesis. Studies such as [74] have stated that collagen deposition seems only to happen on the abluminal side, but the authors of [74] not provide any explanation for this finding.

In stage 2, the intima seems to burst open, as we could observe in some micrographs. Hence, only the media and the adventitia are left, which are not clearly distinguishable anymore. The mechanical behavior becomes very compliant, probably because the stiff intima [75,19] opens. Newly deposited fibers seem to be quite wavy, although we did not quantify the waviness in this study. This might additionally explain the increased distensibility of the wall: as the integrity of the wall decreases, the collagen fibers can straighten and re-orientate without much resistance and get recruited at a later stage with higher stretches compared to healthy arteries or stage 1 AAA walls (see Table 2 and, e.g., Fig. 2, sample AAA 15).

4.1.3. Stage 3

The transition towards stage 3 is associated with a built-up of a significant neo-adventitia. Smaller, disrupted adipocytes are cleaned off by macrophages and only non-disrupted adipocytes remain inside the wall. All walls are common in their stiffness (see, e.g., Fig. 2, sample AAA 2) and a significant amount of neo-adventitia. This neo-adventitia is clearly visible in the intensity plot, exhibiting an increased percentage of the wall having an isotropic fiber orientation with a decreasing percentage of the wall showing fibers oriented towards the circumferential direction.

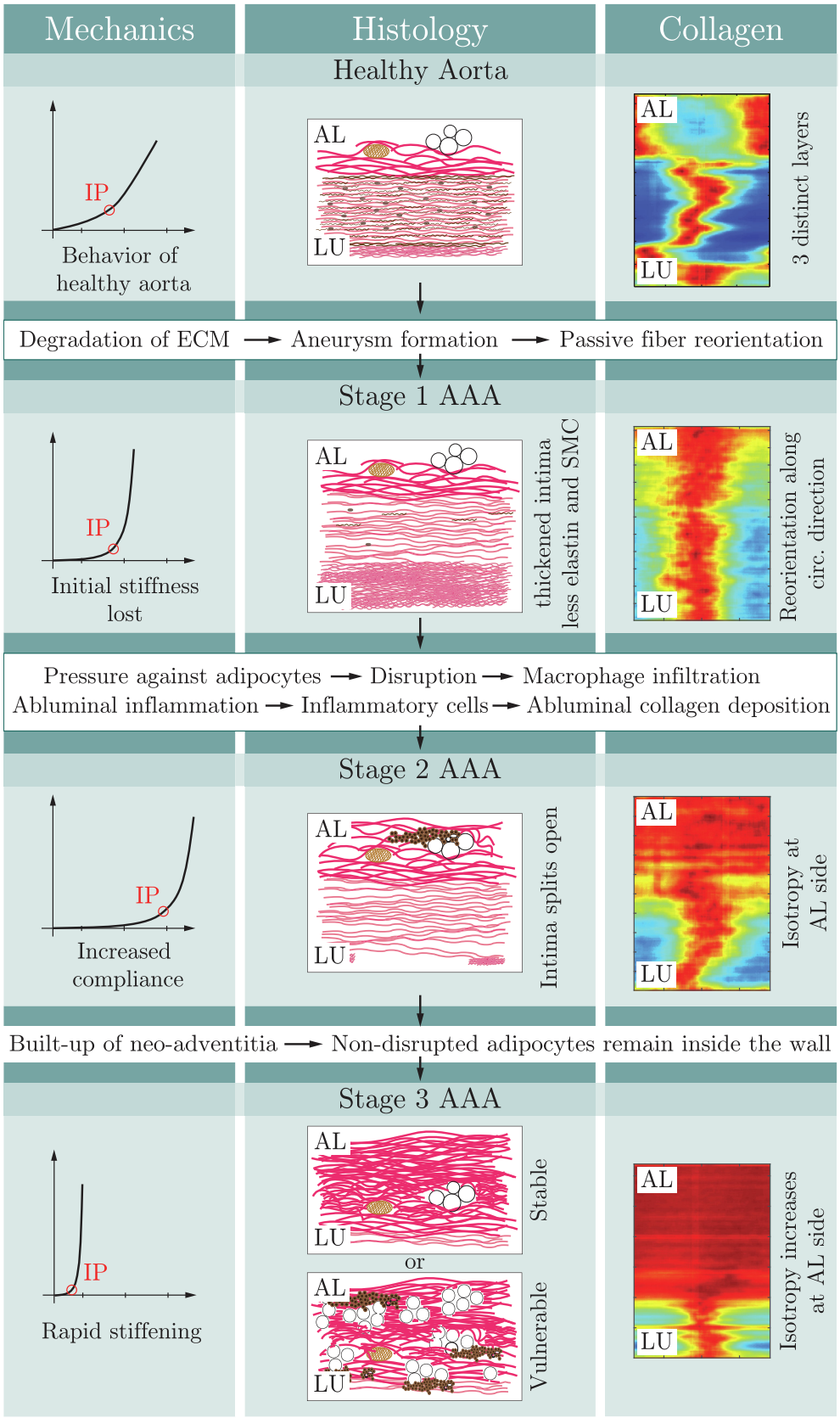

Fig. 7. Flowchart summarizing the disease progression steps, divided into mechanics, histology and collagen, where changes are illustrated between the healthy aorta and three AAA disease stages. The mechanics is illustrated by characteristic stress-stretch curves, showing an idealized mechanical behavior for the respective case and the inflection point (IP) as a red circle. Changes in histology are depicted schematically and color coded as follows: light pink depicts collagen fibers, brown wavy structures symbolize elastin, brown filled circles depicts SMCs, open white circles are adipocytes, brown filled small circles (in Stages 2 and 3) refer to inflammatory cells, and yellow ovals are nerves. The third column of the flowchart, labeled 'Collagen' shows exemplary intensity plots, as explained in Fig. 5. LU = luminal side; AL = abluminal side.

Indeed, in most micrographs no media could be seen anymore and only the adventitia with the newly deposited neo-adventitia remained. This also explains why no significant difference in wall thickness could be seen between the samples, despite of new collagen deposition. Apparently, both intima and media split open, as could be observed on some micrographs. However, to further support this latter theory, a study of whole aneurysms is necessary to confirm the circumferential distribution of the three aortic layers, as unfortunately we only had access to a small piece of AAA walls on the anterior side.

Despite of the common features such as a significant neo-adventitia and no intima nor media are present, we could observe two types of remodeled stage 3 walls. The first type seemed to have remodeled 'safely', see Fig. 6(b). Almost no adipocytes were present inside the wall, only a thick collagen layer was entrapping nerves, which indicated the new collagen deposition. These samples had a higher relative collagen content compared to the other stages (89% and 85%). The second type of walls seemed to have remodeled to a 'vulnerable' state, see Fig. 6 (c). Here, significant amounts of inflammation and adipocytes were visible inside the wall.

Interestingly, we did not see any significant difference in the diameter between the groups, as this measure seems to be unfit as dependent on too many premises. The study [28] examined failure stresses and strains by uniaxial tensile testing and could not find any correlation between failure strains and diameters either.

4.2. Conjunction with the literature

To the authors' knowledge the potentially important role of adipocytes located inside or adjacent to aneurysm walls has been studied by at least two groups: The study [49] applied imaging mass spectrometry to analyze the localization of lipid molecules in human aneurysm walls. The authors of that study discovered that the size of adipocytes was markedly larger compared to those located in the neck, and that the integrity of collagen became disrupted by infiltration of adipocytes. The authors also stated that high plasma triglyceride (TG) levels may be potential risk factors for AAA rupture, however, serum TG levels were not elevated for most of the patients. Their hypothesis was that adipocyte accumulations in AAA walls may be indicators for an increased rupture risk. However, no hypothesis for the origin of the adipocytes was given.

The study [50] performed an animal study with a hyperfusion-induced animal model (developed by the same group and described in [48]) for AAAs and additionally they collected 30 human samples from AAA surgeries. They identified increased amounts of adipocytes in ruptured vessels compared to non-ruptured walls, but did not state whether the adipocytes were included inside the wall or adjacent to the wall. The adipocyte like cells were located in the adventitial side of the AAA sac, but not in the neck in both ruptured and unruptured groups. Additionally they stated that local inflammation was associated with the observed adipocytes. They concluded that the appropriate control of adipocytes may treat or even prevent AAA rupture.

The study [52] examined 20 ruptured and 16 unruptured saccular intracranial aneurysms with respect to lipid accumulations. They identified that intracellular lipid accumulation was associated with wall remodeling and rupture, and that macrophages correlated with these lipid accumulations. Extracellularly, accumulated adipophilin was present in higher amounts in ruptured than unruptured walls, which reflected the death of lipid-laden cells, macrophages and SMCs and the release of their intracellular, adipophilin covered lipids droplets into the ECM. The authors hypothesized that the lipids may originate from the thrombus or from neo-vessels. However, intracranial aneurysms are not surrounded by perivascular fat and hence the mechanism of lipid accumulation is most likely different to the one in AAAs.

Several studies reported remodeling in the adventitia such as [76]. These authors observed significant thickening of the adventitia, accompanied by a recruitment of macrophages. This may highlight an inward progression of inflammation from the adventitia towards the luminal side of the AAA wall. However, they also stated that this is most probably not the first trigger for aneurysm dilatation, as no inflammation in the adventitia was seen in small aneurysms.

The 'tunica adiposa' was described by several groups as a potential source of inflammation. For example, [77,64] connected adipocyte death to macrophages inside the adventitia, and hence to enhanced AAA formation. In addition the study [53] stated that adipocyte tissue, surrounding vessels, might be connected to cellular infiltration of inflammatory cells, and hence play an important factor in an 'outside-in' signaling in the development of diseases such as atherosclerosis and cardiomyopathy. However, the effects of a 'tunica adiposa' around vessels remain incompletely understood and should be examined further [54].

4.3. Conclusion

To the authors' knowledge this is the first study which systematically compares and connects mechanical data from biaxial tensile tests, with histological and structural data to define disease stages. The proposed pathogenesis provides an explanation for contradicting studies stating increased anisotropy, e.g., [29,20,16–18,22], or isotropy, e.g., [78]. According to our hypothesis, collagen in AAA walls realigns passively towards the circumferential direction in the first disease stage, which results in an anisotropic behavior. Subsequently, triggered by inflammation on the abluminal side of the wall, new collagen is deposited isotropically, and hence contributes to a more isotopic behavior. Due to the small sample size no significant differences were identified regarding isotropy or anisotropy, but a trend towards a more isotropic behavior with disease progression could be seen and should be investigated in future studies.

Another key observation was that collagen deposition only occurs in conjunction to infiltration of inflammatory cells. Hence our theory is that no fibers are synthesized without inflammation in the wall and, therefore, no 'safe remodeling' is possible to counteract the lost elasticity due to ECM degeneration. The application of anti-inflammatory drugs might actually be counterproductive and more studies should be employed in this direction, as also stated in [44], referring to [79], which reported a rapid AAA development and rupture in a patient on immunosuppressive drugs. Also [28] suggested that inflammation is not a marker for rupture, but rather for remodeling. Finally, the significant occurrence of adipocytes in potentially 'vulnerable' stage 3 AAA walls might point towards the possibility to image adipocytes inside the wall, even by conventional *ex vivo* imaging techniques such as ultrasound or MRI.

Unfortunately, we were not able to determine the final rupture strength using biaxial tensile tests. Future studies should aim at the determination of biaxial failure properties to better understand the difference in the wall composition of stage 3 AAAs, and whether 'safely' remodeled walls are indeed stronger than 'vulnerable' walls.

As AAAs seem to become first more compliant and then stiffer, monitoring changes in aneurysm distensibility could be a better predictor for rupture that monitoring the change in diameter, as proposed in [80]. These authors deduced that a reduction in distensibility of AAA walls over time was associated with a significantly reduced time until rupture, independent of other risk factors.

To fully understand this progression, there is a need to examine AAA walls on the nano-scale and to closely analyze for collagen undulation and thickness. The impact of diabetes on the mechanics and disease progression should be examined closely in future studies, as we discovered significant differences in the mechanical behavior in diabetes and non-diabetes patients. Additionally we discovered differences in statin intake between the different disease stages, hence the intake of statin should be closely examined in the future, as it may influence AAA growth, as suggested in, e.g., [81–83]. However, no significant correlation between statin intake and adipocytes inside the wall or neo-adventitia growth could be identified in the present study.

Another drawback of our study is of course the small sample size and the limited location from which we gained our samples. Due to patient safety it is not possible for us to gain samples including both sac and neck regions or even whole aneurysms. A future study should aim at gaining whole AAAs from autopsies to confirm the hypothesis that intima and media burst open at a certain point in the disease progression. Last but not least we are hoping that we have motivated new computational growth and remodeling models for the development of AAA, which are able to test our hypothesis of the three stages of aneurysm development.

Funding

This work was supported by BioTechMed-Graz, Austria, to Institute of Biomechanics, in particular ARB.

Conflict of interest

None declared.

Acknowledgement

The authors would like to thank T. Weitlaner and M. Habenbacher for their support in the experimental study. Additionally we would like to thank the Institute of Science and Technology, Klosterneuburg, Austria, for its support in SHG imaging.

References

[1] J.T. Powell, L.C. Brown, The natural history of abdominal aortic aneurysms and their risk of rupture, Acta Chir. Belg. 101 (2001) 11–16.
[2] F.A. Lederle, S.E. Wilson, G.R. Johnson, D.B. Reinke, F.N. Littooy, C.W. Acher, D.J. Ballard, L.M. Messina, I.L. Gordon, E.P. Chute, W.C. Krupski, S.J. Busuttil, G.W. Barone, S. Sparks, L.M. Graham, J.H. Rapp, M.S. Makaroun, G.L. Moneta, R.A. Cambria, R.G. Makhoul, D. Eton, H.J. Ansel, J.A. Freischlag, D. BandykAneurysm Detection and Management Veterans Affairs Cooperative Study Group, Immediate repair compared with surveillance of small abdominal aortic aneurysms, N. Engl. J. Med. 346 (2002) 1437–1444.
[3] M.F. Fillinger, M.L. Raghavan, S.P. Marra, J.L. Cronenwett, F.E. Kennedy, In vivo analysis of mechanical wall stress and abdominal aortic aneurysm rupture risk, J. Vasc. Surg. 36 (2002) 589–597.
[4] C. Fleming, E.P. Whitlock, T.L. Beil, F.A. Lederle, Screening for abdominal aortic aneurysm: a best-evidence systematic review for the U.S. Preventive Services Task Force, Ann. Intern. Med. 142 (2005) 203–211.
[5] N. Sakalihasan, R. Limet, O.D. Defawe, Abdominal aortic aneurysm, Lancet 365 (2005) 1577–1589.
[6] D.A. Vorp, J.P. Vande Geest, Biomechanical determinants of abdominal aortic aneurysm rupture, Arterioscler. Thromb. Vasc. Biol. 25 (2005) 1558–1566.
[7] D.C. Brewester, J.L. Cronenwett, J.W. Hallett Jr., K.W. Johnston, W.C. Krupski, J.S. Matsumura, Guidelines for the treatment of abdominal aortic aneurysms. Report of a subcommittee of joint council of the american association of vascular surgery and society of vascular surgery, J. Vasc. Surg. 37 (2003) 1106–1117.
[8] J. Stenbaek, B. Kalin, J. Swedenborg, Growth of thrombus may be a better predictor of rupture than diameter in patients with abdominal aortic aneurysms, Eur. J. Vasc. Endovasc. Surg. 20 (2000) 466–499.
[9] B.J. Doyle, A. Callanan, P.E. Burke, P.A. Grace, M.T. Walsh, D.A. Vorp, T.M. McGloughlin, Vessel asymmetry as an additional diagnostic tool in the assessment of abdominal aortic aneurysms, J. Vasc. Surg. 49 (2009) 443–454.
[10] D.H.J. Wang, M.S. Makaroun, M.W. Webster, D.A. Vorp, Effect of intraluminal thrombus on wall stress in patient-specific models of abdominal aortic aneurysm, J. Vasc. Surg. 36 (2002) 598–604.
[11] Z. Li, C. Kleinstreuer, A new wall stress equation for aneurysm-rupture prediction, Ann. Biomed. Eng. 33 (2005) 209–213.
[12] A.H. Malkawi, R.J. Hinchliffe, Y. Xu, P.J. Holt, I.M. Loftus, M.M. Thompson, Patient-specific biomechanical profiling in abdominal aortic aneurysm development and rupture, J. Vasc. Surg. 52 (2010) 480–488.
[13] G.A. Holzapfel, J. Tong, T. Cohnert, P. Regitnig, Recent advances in the biomechanics of abdominal aortic aneurysms, in: N. Chakfé, B. Durand, W. Meichelboeck (Eds.), ESVB 2011 New Endovascular Technologies, From Bench Test to Clinical Practice, Europrot, Strasbourg, France, 2011, pp. 23–40.
[14] J.D. Humphrey, Cardiovascular Solid Mechanics. Cells, Tissues, and Organs, Springer-Verlag, New York, 2002.
[15] M.L. Raghavan, D.A. Vorp, M.P. Federle, M.S. Makaroun, M.W. Webster, Wall stress distribution on three-dimensionally reconstructed models of human abdominal aortic aneurysm, J. Vasc. Surg. 31 (2000) 760–769.
[16] J.P. Vande Geest, M.S. Sacks, D.A. Vorp, The effects of aneurysm on the biaxial mechanical behavior of human abdominal aorta, J. Biomech. 39 (2006) 1324–1334.
[17] J. Tong, T. Cohnert, P. Regitnig, G.A. Holzapfel, Effects of age on the elastic properties of the intraluminal thrombus and the thrombus-covered wall in abdominal aortic aneurysms: biaxial extension behavior and material modeling, Eur. J. Vasc. Endovasc. Surg. 42 (2011) 207–219.
[18] S.A. O'Leary, E.G. Kavanagh, P.A. Grace, T.M. McGloughlin, B.J. Dolye, The biaxial mechanical behaviour of abdominal aortic aneurysm intraluminal thrombus: classification of morphology and the determination of layer and region specific properties, J. Biomech. 47 (2014) 1430–1437.
[19] J.A. Niestrawska, Ch. Viertler, P. Regitnig, T.U. Cohnert, G. Sommer, G.A. Holzapfel, Microstructure and mechanics of healthy and aneurysmatic abdominal aortas: experimental analysis and modeling, J.R. Soc. Interface 13 (2016). 20160620.
[20] M.J. Thubrikar, M. Labrosse, F. Robicsek, J. Al-Soudi, B. Fowler, Mechanical properties of abdominal aortic aneurysm wall, J. Med. Eng. Technol. 25 (2001) 133–142.
[21] D.M. Pierce, T.E. Fastl, B. Rodriguez-Vila, P. Verbrugghe, I. Fourneau, G. Maleux, P. Herijgers, E.J. Gomez, G.A. Holzapfel, A method for incorporating three-dimensional residual stretches/stresses into patient-specific finite element simulations of arteries, J. Mech. Behav. Biomed. Mater. 47 (2015) 147–164.
[22] S.G. Sassani, J. Kakisis, S. Tsangaris, D.P. Sokolis, Layer-dependent wall properties of abdominal aortic aneurysms: experimental study and material characterization, J. Mech. Behav. Biomed. Mater. 49 (2015) 141–161.
[23] C.M. He, M.R. Roach, The composition and mechanical properties of abdominal aortic aneurysms, J. Vasc. Surg. 20 (1994) 6–13.
[24] E.S. Di Martino, A. Bohra, J.P. Vande Geest, N.Y. Gupta, M.S. Makaroun, D.A. Vorp, Biomechanical properties of ruptured versus electively repaired abdominal aortic aneurysm wall tissue, J. Vasc. Surg. 43 (2006) 570–576.
[25] M.L. Raghavan, J. Kratzberg, E.M. Castro de Tolosa, M.M. Hanaoka, P. Walker, E. S. da Silva, Regional distribution of wall thickness and failure properties of human abdominal aortic aneurysm, J. Biomech. 39 (2006) 3010–3016.
[26] M.L. Raghavan, M.M. Hanaoka, J.A. Kratzberg, M. de Lourdes Higuchi, E.S. da Silva, Biomechanical failure properties and microstructural content of ruptured and unruptured abdominal aortic aneurysms, J. Biomech. 44 (2011) 2501–2507.
[27] C. Forsell, J. Swedenborg, J. Roy, T.C. Gasser, The quasi-static failure properties of the abdominal aortic aneurysm wall estimated by a mixed experimental-numerical approach, Ann. Biomed. Eng. 41 (2013) 1554–1566.
[28] J.A. Tavares Monteiro, E.S. da Silva, M.L. Raghavan, P. Puech-Leão, M. de Lourdes Higuchi, J.P. Otoch, Histologic, histochemical, and biomechanical properties of fragments isolated from the anterior wall of abdominal aortic aneurysms, J. Vasc. Surg. 59 (2014) 1393–1401.
[29] D.S. Sumner, D.E. Hokanson, D.E. Strandness Jr., Stress-strain characteristics and collagen-elastin content of abdominal aortic aneurysms, Surg. Gynecol. Obstet. 130 (1970) 459–466.
[30] S.T. MacSweeney, G. Young, R.M. Greenhalgh, J.T. Powell, Mechanical properties of the aneurysmal aorta, Br. J. Surg. 79 (1992) 1281–1284.
[31] S. Polzer, T.C. Gasser, K. Novak, V. Man, M. Tichy, P. Skacel, J. Bursa, Structure-based constitutive model can accurately predict planar biaxial properties of aortic wall tissue, Acta Biomater. 14 (2015) 133–145.
[32] A.M. Robertson, X. Duan, K.M. Aziz, M.R. Hill, S.C. Watkins, J.R. Cebral, Diversity in the strength and structure of unruptured cerebral aneurysms, Ann. Biomed. Eng. 43 (2015) 1502–1515.
[33] M. Carmo, L. Colombo, A. Bruno, F.R. Corsi, L. Roncoroni, M.S. Cuttin, F. Radice, E. Mussini, P.G. Settembrini, Alteration of elastin, collagen and their cross-links in abdominal aortic aneurysms, Eur. J. Vasc. Endovasc. Surg. 23 (2002) 543–549.
[34] D.A. Vorp, Biomechanics of abdominal aortic aneurysm, J. Biomech. 40 (2007) 1887–1902.
[35] J.H. Lindeman, B.A. Ashcroft, J.W. Beenakker, M. van Es, N.B. Koekkoek, F.A. Prins, J.F. Tielemans, H. Abdul-Hussien, R.A. Bank, T.H. Oosterkamp, Distinct defects in collagen microarchitecture underlie vessel-wall failure in advanced abdominal aneurysms and aneurysms in Marfan syndrome, Proc. Natl. Acad. Sci. USA 107 (2010) 862–865.
[36] T.C. Gasser, S. Gallinetti, X. Xing, C. Forsell, J. Swedenborg, J. Roy, Spatial orientation of collagen fibers in the abdominal aortic aneurysm's wall and its relation to wall mechanics, Acta Biomater. 8 (2012) 3091–3103.

[37] P.B. Dobrin, W.H. Baker, W.C. Gley, Elastolytic and collagenolytic studies of arteries. Implications for the mechanical properties of aneurysms, Arch. Surg. 119 (1984) 405–409.
[38] K.A. Wilson, J.S. Lindholt, P.R. Hoskins, L. Heickendorff, S. Vammen, A.W. Bradbury, The relationship between abdominal aortic aneurysm distensibility and serum markers of elastin and collagen metabolism, Eur. J. Vasc. Endovasc. Surg. 21 (2001) 175–178.
[39] S. Menashi, J.S. Campa, R.M. Greenhalgh, J.T. Powell, Collagen in abdominal aortic aneurysm: typing, content, and degradation, J. Vasc. Surg. 6 (1987) 578–582.
[40] R.J. Rizzo, W.J. McCarthy, S.N. Dixit, M.P. Lilly, V.P. Shively, W.R. Flinn, J.S. Yao, Collagen types and matrix protein content in human abdominal aortic aneurysms, J. Vasc. Surg. 10 (1989) 365–373.
[41] G.S. McGee, B.T. Baxter, V.P. Shively, R. Chisholm, W.J. McCarthy, W.R. Flinn, J.S. Yao, W.H. Pearce, Aneurysm or occlusive disease-factors determining the clinical course of atherosclerosis of the infrarenal aorta, Surgery 110 (1991) 370–375.
[42] B.T. Baxter, G.S. McGee, V.P. Shively, I.A. Drummond, S.N. Dixit, M. Yamauchi, W.H. Pearce, Elastin content, cross-links, and mRNA in normal and aneurysmal human aorta, J. Vasc. Surg. 16 (1992) 192–200.
[43] R.H. Gandhi, E. Irizarry, J.O. Cantor, S. Keller, G.B. Nackman, V.J. Halpern, K.M. Newman, M.D. Tilson, Analysis of elastin cross-linking and the connective tissue matrix of abdominal aortic aneurysms, Surgery 115 (1994) 617–620.
[44] H. Kuivaniemi, E.J. Ryer, J.R. Elmore, G. Tromp, Understanding the pathogenesis of abdominal aortic aneurysms, Expert Rev. Cardiovasc. Ther. 13 (2015) 975–987.
[45] N. Sakalihasan, H. Kuivaniemi, B. Nusgens, R. Durieux, J.-O. Defraigne, Aneurysm: epidemiology aetiology and pathophysiology, in: T.M. McGloughlin (Ed.), Biomechanics and mechanobiology of aneurysms, Springer, New York, 2010, pp. 1–33.
[46] J.A. Curci, R.W. Thompson, Adaptive cellular immunity in aortic aneurysms: cause, consequence, or context?, J Clin. Invest. 114 (2004) 168–171.
[47] M.H. Ross, W. Pawlina, Histology: A Text and Atlas: with Correlated Cell and Molecular Biology, sixth ed., Lippincott Williams & Wilkins, 2011.
[48] H. Tanaka, N. Zaima, T. Sasaki, M. Sano, N. Yamamoto, T. Saito, K. Inuzuka, T. Hayasaka, N. Goto-Inoue, Y. Sugiura, K. Sato, H. Kugo, T. Moriyama, H. Konno, M. Setou, N. Unno, Hypoperfusion of the adventitial vasa vasorum develops an abdominal aortic aneurysm, PLoS One 10 (2015). 0 0134386.
[49] H. Tanaka, N. Zaima, T. Sasaki, N. Yamamoto, K. Inuzuka, M. Sano, T. Saito, T. Hayasaka, N. Goto-Inoue, K. Sato, H. Kugo, T. Moriyama, H. Konno, M. Setou, N. Unno, Imaging mass spectrometry reveals a unique distribution of triglycerides in the abdominal aortic aneurysmal wall, J. Vasc. Res. 52 (2015) 127–135.
[50] H. Kugo, N. Zaima, H. Tanaka, Y. Mouri, K. Yanagimoto, K. Hayamizu, K. Hashimoto, T. Sasaki, M. Sano, T. Yata, T. Urano, M. Setou, N. Unno, T. Moriyama, Adipocyte in vascular wall can induce the rupture of abdominal aortic aneurysm, Sci. Rep. 6 (2016). 0 31268.
[51] H. Kugo, N. Zaima, H. Tanaka, K. Hashimoto, C. Miyamoto, A. Sawaragi, T. Urano, N. Unno, T. Moriyama, Pathological analysis of the ruptured vascular wall of hypoperfusion-induced abdominal aortic aneurysm animal model, J. Orthop. Sc. 66 (2017) 499–506.
[52] E. Ollikainen, R. Tulamo, S. Lehti, M. Lee-Rueckert, J. Hernesniemi, M. Niemelä, S. Ylä-Herttuala, P.T. Kovanen, J. Frösen, Smooth muscle cell foam cell formation, apolipoproteins, and ABCA1 in intracranial aneurysms: implications for lipid accumulation as a promoter of aneurysm all rupture, J. Neuropath. Exp. Neur. 75 (2016) 689–699.
[53] G.N. Chaldakov, Cardiovascular adipobiology: a novel heart-associated adipose tissue in cardiovascular disease, Ser. J. Exp. Clin. Res. 9 (2008) 81–88.
[54] K.A. Britton, C.S. Fox, Perivascular adipose tissue and vascular disease, Clin. Lipidol. 6 (2011) 79–91.
[55] A.J. Schriefl, H. Wolinski, P. Regitnig, S.D. Kohlwein, G.A. Holzapfel, An automated approach for three-dimensional quantification of fibrillar structures in optically cleared soft biological tissues, J.R. Soc. Interface 10 (2013). 20120760.
[56] G. Sommer, D.C. Haspinger, M. Andrä, M. Sacherer, Ch. Viertler, P. Regitnig, G.A. Holzapfel, Quantification of shear deformations and corresponding stresses in the biaxially tested human myocardium, Ann. Biomed. Eng. 43 (2015) 2234–2348.
[57] G.A. Holzapfel, Nonlinear Solid Mechanics. A Continuum Approach for Engineering, John Wiley & Sons, Chichester, 2000.
[58] G.A. Holzapfel, J.A. Niestrawska, R.W. Ogden, A.J. Reinisch, A.J. Schriefl, Modelling non-symmetric collagen fibre dispersion in arterial walls, J.R. Soc. Interface 12 (2015). 20150188.
[59] A.J. Schriefl, G. Zeindlinger, D.M. Pierce, P. Regitnig, G.A. Holzapfel, Determination of the layer-specific distributed collagen fiber orientations in human thoracic and abdominal aortas and common iliac arteries, J.R. Soc. Interface 9 (2012) 1275–1286.
[60] The MathWorks inc., MATLAB R2016a, Natick, MA, USA, 2016.
[61] A. Wittek, W. Derwich, C.-P. Fritzen, T. Schmitz-Rixen, C. Blase, Towards non-invasive in vivo characterization of the pathophysiological state and mechanical wall strength of the individual human AAA wall based on 4D ultrasound measurements, Z. Angew. Math. Mech. 98 (2018) 2275–2294.
[62] S.S. Hans, O. Jareunpoon, M. Balasubramaniam, G.B. Zelenock, Size and location of thrombus in intact and ruptured abdominal aortic aneurysms, J. Vasc. Surg. 41 (2005) 584–588.
[63] N. Grootenboer, J.L. Bosch, J.M. Hendriks, M.R. van Sambeek, Epidemiology, aetiology, risk of rupture and treatment of abdominal aortic aneurysms: does sex matter?, Eur J. Vasc. Endovasc. Surg. 38 (2009) 278–284.
[64] S.B. Police, S.E. Thatcher, R. Charnigo, A. Daugherty, L.A. Cassis, Obesity promotes inflammation in periaortic adipose tissue and angiotensin II-induced abdominal aortic aneurysm formation, Arterioscler. Thromb. Vasc. Biol. 29 (2009) 1458–1464.
[65] C.M. Brophy, J.M. Reilly, G.J.W. Smith, M.D. Tilson, The role of inflammation in nonspecific abdominal aortic aneurysm disease, Ann. Vasc. Surg. 5 (1991) 229–233.
[66] N. Sakalihasan, A. Heyeres, B.V. Nusgens, R. Limet, C.M. Lapiére, Modifications of the extracellular matrix of aneurysmal abdominal aortas as a function of their size, Eur. J. Vasc. Surg. 7 (1993) 633–637.
[67] E.L. Henderson, Y. Geng, G.K. Sukhova, A.D. Whittemore, J. Knox, P. Libby, Death of smooth muscle cells and expression of mediators of apoptosis by T lymphocytes in human abdominal aortic aneurysms, Circulation 99 (1999) 96–104.
[68] K. Shimizu, R.N. Mitchell, P. Libby, Inflammation and cellular immune responses in abdominal aortic aneurysms, Arterioscler. Thromb. Vasc. Biol. 26 (2006) 987–994.
[69] J.V. White, K. Haas, S. Phillips, A.J. Comerota, Adventitial elastolysis is a primary event in aneurysm formation, J. Vasc. Surg. 17 (1993) 371–380.
[70] S. Galic, J.S. Oakhill, G.R. Steinberg, Adipose tissue as an endocrine organ, Mol. Cell. Endocrinol. 316 (2010) 129–139.
[71] K. Karastergiou, V. Mohamed-Ali, The autocrine and paracrine roles of adipokines, Mol. Cell. Endocrinol. 318 (2010) 69–78.
[72] T. Tsuruda, J. Kato, K. Hatakeyama, K. Kojima, M. Yano, Y. Yano, K. Nakamura, F. Nakamura-Uchiyama, Y. Matsushima, T. Imamura, T. Onitsuka, Y. Asada, Y. Nawa, T. Eto, K. Kitamura, Adventitial mast cells contribute to pathogenesis in the progression of abdominal aortic aneurysm, Circ. Res. 102 (2008) 1368–1377.
[73] H. Åstrand, Å. Rydén-Ahlgren, T. Sandgren, T. Länne, Age-related increase in wall stress of the human abdominal aorta: an in vivo study, J. Vasc. Surg. 42 (2005) 926–931.
[74] T. Tsuruda, T. Imamura, K. Hatakeyama, Y. Asada, K. Kitamura, Stromal cell biology-a way to understand the evolution of cardiovascular diseases, Circ. J. 74 (2010) 1042–1050.
[75] H. Weisbecker, D.M. Pierce, P. Regitnig, G.A. Holzapfel, Layer-specific damage experiments and modeling of human thoracic and abdominal aortas with non-atherosclerotic intimal thickening, J. Mech. Behav. Biomed. Mater. 12 (2012) 93–106.
[76] K. Maiellaro, W.R. Taylor, The role of the adventitia in vascular inflammation, Cardiovasc. Res. 75 (2007) 640–648.
[77] S. Cinti, G. Mitchell, G. Barbatelli, I. Murano, E. Ceresi, E. Faloia, S. Wang, M. Fortier, A.S. Greenberg, M.S. Obin, Adipocyte death defines macrophage localization and function in adipose tissue of obese mice and humans, J. Lipid Res. 46 (2005) 2347–2355.
[78] M.L. Raghavan, M.W. Webster, D.A. Vorp, Ex vivo biomechanical behavior of abdominal aortic aneurysm: assessment using a new mathematical model, Ann. Biomed. Eng. 24 (1996) 573–582.
[79] J.H. Lindeman, T.J. Rabelink, J.H. van Bockel, Immunosuppression and the abdominal aortic aneurysm: Doctor Jekyll or Mister Hyde?, Circulation 124 (2011) e463–e465
[80] K.A. Wilson, A.J. Lee, P.R. Hoskins, F.G. Fowkes, C.V. Ruckley, A.W. Bradbury, The relationship between aortic wall distensibility and rupture of infrarenal abdominal aortic aneurysm, Eur. J. Vasc. Endovasc. Surg. 37 (2003) 112–117.
[81] E.F. Steinmetz, C. Buckley, M.L. Shames, T.L. Ennis, S.J. Vanvickle-Chavez, D. Mao, L.A. Goeddel, C.J. Hawkins, R.W. Thompson, Treatment with simvastatin suppresses the development of experimental abdominal aortic aneurysms in normal and hypercholesterolemic mice, Ann. Surg. 241 (2005) 92–101.
[82] A. Kalyanasundaram, J.R. Elmore, J.R. Manazer, A. Golden, D.P. Franklin, S.W. Galt, E.M. Zakhary, D.J. Carey, Simvastatin suppresses experimental aortic aneurysm expansion, J. Vasc. Surg. 43 (2006) 117–124.
[83] R. Hurks, I.E. Hoefer, A. Vink, G. Pasterkamp, A. Schoneveld, M. Kerver, J.P. de Vries, M.J. Tangelder, F.L. Moll, Different effects of commonly prescribed statins on abdominal aortic aneurysm wall biology, Eur. J. Vasc. Endovasc. Surg. 39 (2010) 569–576.